Electronic Supplementary Material (ESI) for Journal of Materials Chemistry A.
This journal is © The Royal Society of Chemistry 2024

SUPPORTING INFORMATION

High responsivity and stability of MSM structured MoS_2 photodetectors by remote hydrogen plasma treatment and alternating growth of Al_2O_3/HfO_2 passivation layers

Yulin Li[a], Yajun Tian[a], Lingjie Bao[a], Haoran Cheng[a,*] and Qijin Cheng[a,*]

[a)] School of Electronic Science and Engineering, Xiamen University, Xiamen, 361102, P. R. China.

*Corresponding author. Tel: +86592-2188342

E-mail address: qijin.cheng@xmu.edu.cn（Qijin Cheng）

chr0247@gmail.com（Haoran Cheng）

Supporting Note 1: The photographs of the MSM structured MoS_2

photodetector before and after passivation of Al_2O_3/HfO_2.

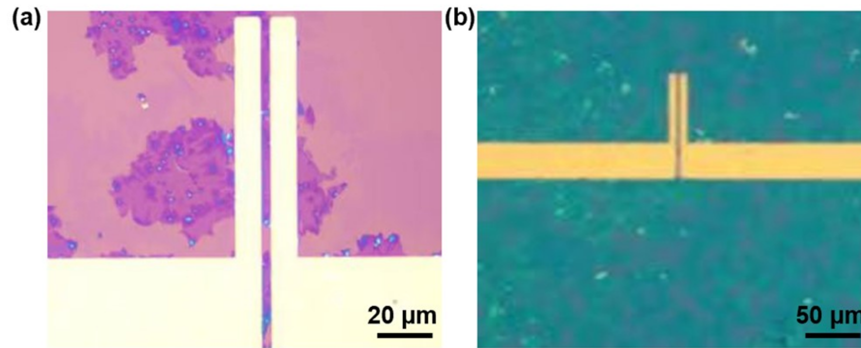

Fig. S1 Optical microscope images of (a) the MSM structured MoS_2 photodetector and (b) the MSM structured MoS_2 photodetector with 20 nm alternating grown Al_2O_3/HfO_2 passivation layers.

Supporting Note 2: The photocurrent and dark current of the pristine MoS_2 photodetector (Device A) before and after the passivation of Al_2O_3/HfO_2.

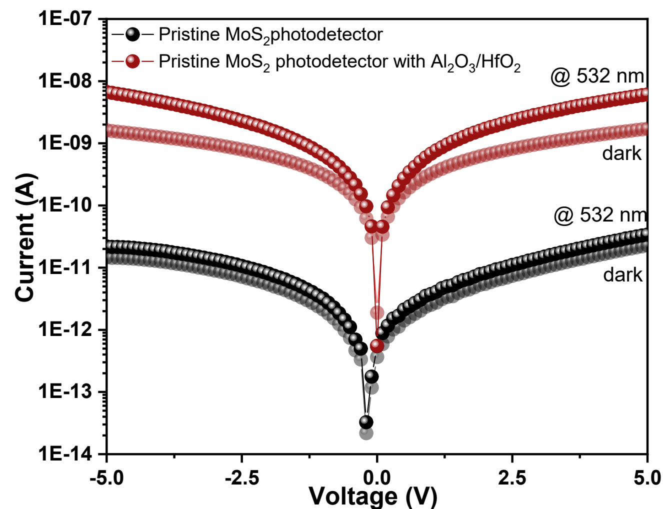

Fig. S2 Current-voltage characteristic curves of the pristine MoS_2 photodetector before and after the passivation of Al_2O_3/HfO_2 under dark condition and 532 nm light illumination.

From Fig. S2, one can notice that, after the passivation of Al_2O_3/HfO_2, both the photocurrent and dark current of the pristine MoS_2 photodetector increase. The increase of the photocurrent and the dark current may be related to the following factors: (i) Al_2O_3/HfO_2 passivation reduces the Schottky barrier height between the metal electrode

and MoS_2, which can increase the possibility of tunneling process and thermionic emission process; (ii) Al_2O_3/HfO_2 passivation effectively separates water and oxygen molecules from the surface of MoS_2, and creates additional conduction pathways through electrostatic doping of fixed positive charges on the MoS_2 surface; (iii) the suppression of Coulomb scattering in MoS_2 after deposition of high-k dielectric materials.

Supporting Note 3: Performance comparison of Device B and Device C before and after two months of placement in the atmosphere environment.

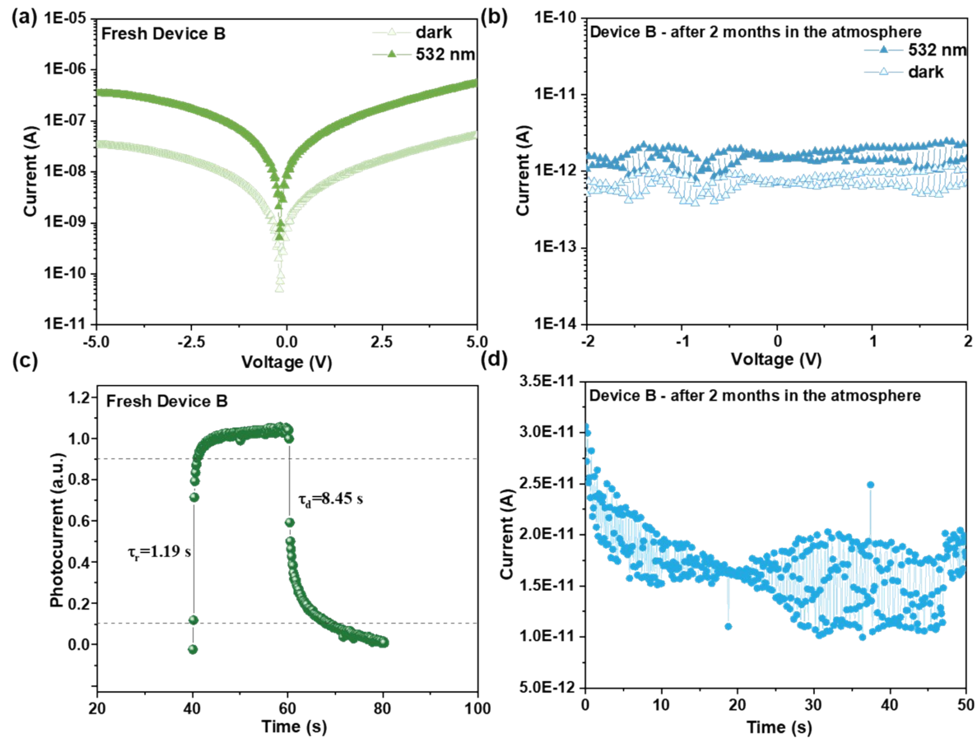

Fig. S3 I-V characteristic curves of (a) fresh Device B and (b) Device B after 2 months of placement in the atmospheric environment under dark condition and 532 nm light illumination. One-cycle time-dependent photoresponses of (c) fresh Device B and (d) Device B after 2 months of placement in the atmospheric environment under 532 nm light illumination. In order to facilitate observation and calculation of 10%-90% response time, only the data between 40-80s points are retained in the figure.

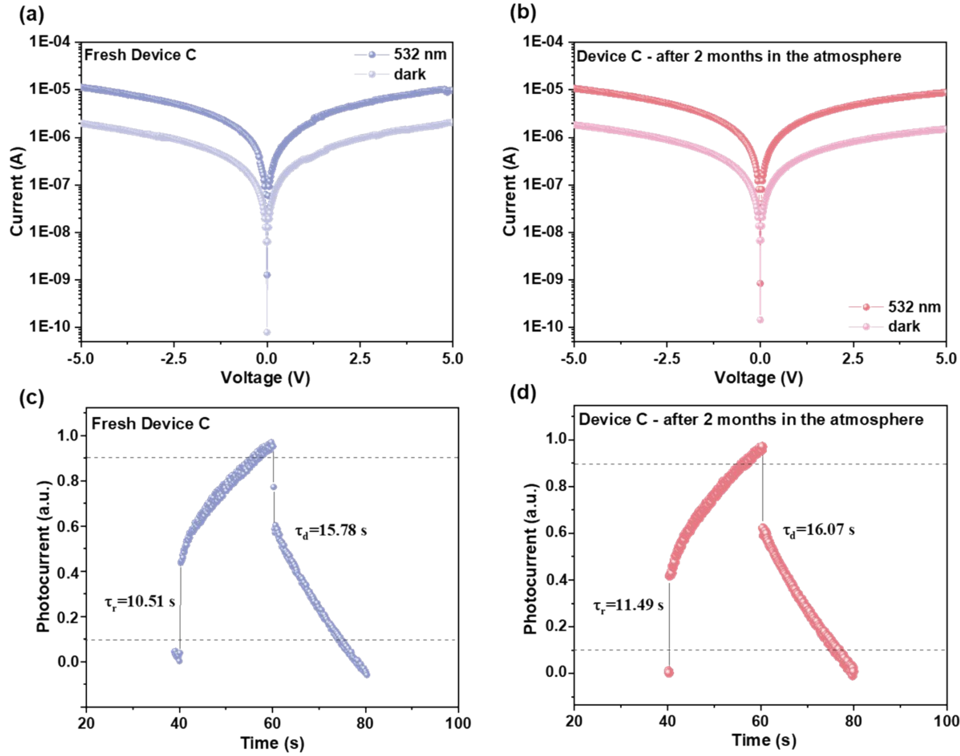

Fig. S4 I-V characteristic curves of (a) fresh Device C and (b) Device C after two months of placement in the atmospheric environment under dark condition and 532 nm light illumination. One-cycle time-dependent photoresponses of (c) fresh Device C and (d) Device C after two months of placement in the atmospheric environment under 532 nm light illumination. In order to facilitate observation and calculation of 10%-90% response time, only the data between 40-80s points are retained in the figure.

From Fig. S3a-d, one can notice that, after being exposed to the atmospheric environment for two months, Device B has completely lost its photoresponse characteristics. The current-voltage characteristic curve and one-cycle time-dependent photoresponse of Device B after being placed in the atmospheric environment for 2 months can not be tested as shown in Fig. S3c and d. From Fig. S4a-d, it can be observed that, after 2 months of placement in the atmospheric environment, Device C shows negligible change in both the photocurrent and the dark current, remaining the same order of magnitude as the fresh device. Through formulas $R_\lambda = \frac{I_{ph}}{A * P}$ and $D^* \approx \frac{\sqrt{A}R_\lambda}{\sqrt{2eI_{dark}}}$, we can determine that the responsivity and the specific detectivity of

Device C after being placed in the atmospheric environment for 2 months are 540.61 A/W and 1.06×10^{10} Jones at a bias of -5 V, respectively. The responsivity and the specific detectivity are maintained at approximately 95% of the fresh Device C. From Fig. S4d, one can notice that the response time (τ_r/τ_d) of Device C after being placed in the atmospheric environment for 2 months is 11.49/16.07 s. In comparison with the fresh Device C, the response time slightly increases.

Supporting Note 4: Photoelectric performance of five fabricated photodetectors under the same condition as Device C before and after 2 months of placement in atmospheric environment

In order to further substantiate the stability and repeatability of the fabricated MoS_2 photodetectors, we have fabricated five photodetectors under the same condition as Device C and measured their photoelectric performance. We have listed the responsivity and specific detectivity of these five photodetectors before and after 2 months of placement in atmospheric environment in Tables S1. The responsivity and specific detectivity were also calculated at bias of -5 V under 532 nm light illumination. From Table S1, the average values of the responsivity and specific detectivity of these fresh devices are 559.82 A/W and 1.19×10^{10} Jones, respectively. The standard deviations of responsivity and specific detectivity of these fresh devices are 13.09 A/W and 1.10×10^9 Jones, respectively. The average values of the responsivity and specific detectivity of these devices after two months of placement in the atmospheric environment are 532.36 A/W and 1.13×10^{10} Jones, respectively. The standard deviations of responsivity and specific detectivity of these devices after two months of placement in the atmospheric environment are 12.73 A/W and 1.13×10^9 Jones, respectively. Our results indicate that Device C is highly reproducible.

Table S1. Responsivity and specific detectivity of the fabricated five photodetectors under the same condition as Device C before and after 2 months of placement in atmospheric environment

Device	Responsivity	Specific detectivity	Responsivity	Specific detectivity

	(A/W)	(Jones)	(A/W)	(Jones)
	Fresh		2 months in atmosphere	
Device 1	567.00	1.12×10^{10}	540.61	1.06×10^{10}
Device 2	537.16	1.32×10^{10}	510.42	1.28×10^{10}
Device 3	572.34	1.06×10^{10}	544.66	1.02×10^{10}
Device 4	553.25	1.30×10^{10}	525.67	1.25×10^{10}
Device 5	569.37	1.09×10^{10}	540.43	1.03×10^{10}

Supporting Note 5: Electrical properties of alternating grown Al_2O_3/HfO_2 passivation layers.

In this work, the electrical properties of alternating grown Al_2O_3/HfO_2 passivation layers (abbreviated as AGAHPLs here) also play a significant role in the performance of the MoS_2 photodetector. Therefore, we fabricated a Ti/Cu/AGAHPLs/p^+-Si metal-oxide-semiconductor (MOS) capacitor to obtain the electrical properties of AGAHPLs (the schematic diagram of the capacitor's structure is shown in Fig. S5a). The capacitance-voltage (C-V) characteristic curve of the Ti/Cu/AGAHPLs/p^+-Si MOS capacitor is shown in Fig. S5b. In Fig. S5b, V_{fb} represents the flat-band voltage of the semiconductor surface energy band, which is used to eliminate the influence of oxide layers and interface charges[1]. It is an essential parameter for determining the polarity of fixed charges. V_{fb} is determined by the abscissa value corresponding to C_{fb}. C_{fb} can be calculated using the following formula[2]:

$$C_{fb} = C_{ox} \Big/ \left(1 + \frac{\varepsilon_{ox}}{\varepsilon_s t_{ox}} \sqrt{\frac{\kappa T \varepsilon_0 \varepsilon_s}{e^2 N_A}}\right) \quad (1)$$

where C_{ox} is the capacitance of the gate oxide (C_{ox}=C_{max}=1.435 nF as shown in Fig. S5b); ε_s is the relative dielectric constant of p^+-Si (ε_s=11.9); t_{ox} is the total thickness of the oxide layer (t_{ox}=20 nm in this work, as shown in Fig. S5c and d); k is the Boltzmann constant (k=1.38×10^{-23} J/K); T is the absolute temperature (T=300 K); ε_0 is the vacuum dielectric constant (ε_0=8.85×10^{-12} F/m); e is the

elementary charge (e=1.602×10^{-19} C); N_A is the p$^+$-Si doping concentration (N_A≈10^{19} cm^{-3} in this work); ε_{ox} is the relative dielectric constant of AGAHPLs (calculated from the formula $C_{ox} = A\frac{\varepsilon_0 \varepsilon_{ox}}{t_{ox}}$, where A is the area of metal electrodes (A=0.25×10^{-6} m^2 in this work), giving rise to ε_{ox}=12.97). According to Equation (1), the calculated C_{fb} is 1.340 nF, corresponding to V_{fb} of -1.682 V, as shown in Fig. S5b.

Based on the obtained electrical parameters of the Ti/Cu/AGAHPLs/p$^+$-Si capacitor from the above analysis, we can determine the fixed oxide charge density (Q_{ox}) of alternating grown Al_2O_3/HfO_2 passivation layers using the following formula[3, 4]:

$$Q_{ox} = \frac{-C_{ox}(V_{fb} + V_{ms})}{eA} \qquad (2)$$

where V_{ms} is the contact potential difference between the metal (Ti) and the p$^+$ Si ($V_{ms} = \frac{W_s - W_m}{e} = \frac{5.23\ eV - 4.33\ eV}{e} = 0.9\ V$). According to Equation (2), the calculated Q_{ox} for AGAHPLs is 2.801×10^{12} cm^{-2}, higher than Q_{ox} for SiO_2 (~10^{10} cm^{-2})[5]. Both the negative V_{fb} and the positive Q_{ox} indicate that alternating grown Al_2O_3/HfO_2 passivation layers carry high fixed positive charges[6].

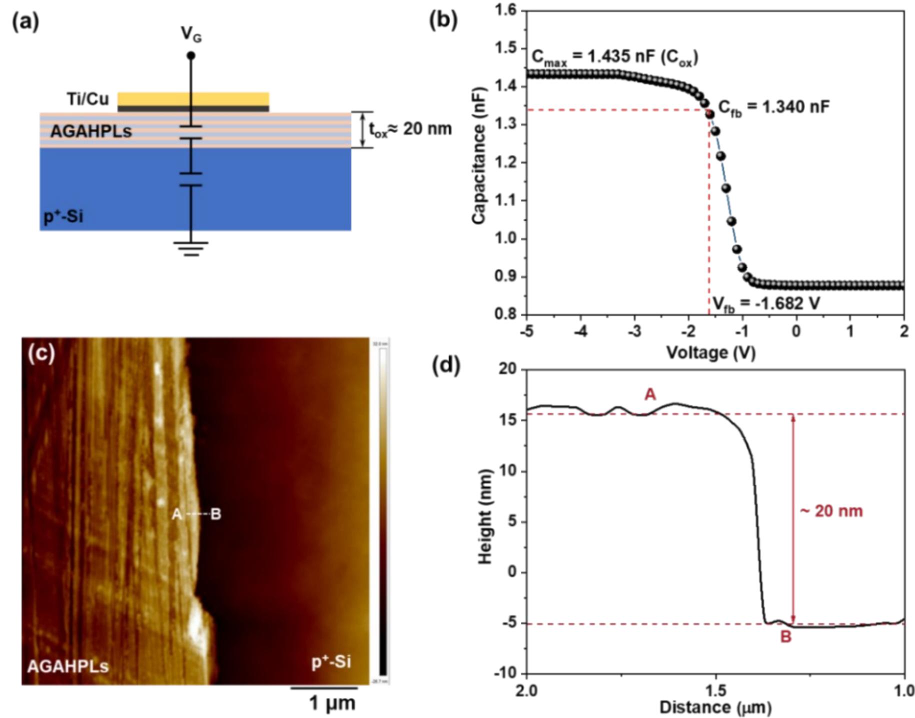

Fig. S5 (a) Schematic diagram of the Ti/Cu/AGAHPLs/p$^+$-Si MOS capacitor's structure. (b) C-V characteristic curve of the Ti/Cu/AGAHPLs/p$^+$-Si MOS capacitor. (c) AFM image of AGAHPLs. (d) AFM height profile between point A and point B shown in Fig. S5c.

References

1. J. Fan, H. Liu, Q. Kuang, B. Gao, F. Ma and Y. Hao, *Microelectron. Reliab.*, 2012, **52**, 1043.
2. L. Hao, G. He, G. Zheng, Q. Gao, L. Qiao and Z. Fang, *ACS Appl. Electron. Mater.*, 2021, **3**, 872.
3. L. Hao, G. He, Z. Fang, D. Wang, Z. Sun and Y. Liu, *Appl. Surf. Sci.*, 2020, **508**, 145273.
4. H. J. Quah, W. F. Lim, K. Y. Cheong, Z. Hassan and Z. Lockman, *J. Cryst. Growth*, 2011, **326**, 2.
5. H. Wong and H. Iwai, *Microelectron. Eng.*, 2006, **83**, 1867.
6. M. Shahinur Rahman, E. K. Evangelou, N. Konofaos and A. Dimoulas, *J. Appl. Phys.*, 2012, **112**, 094501